Dalton Transactions

PAPER

View Article Online
View Journal | View Issue

Cite this: *Dalton Trans.*, 2015, **44**, 1805

Electronic structure of β-RbSm$(MoO_4)_2$ and chemical bonding in molybdates†

V. V. Atuchin,*[a,b,c] A. S. Aleksandrovsky,[d,e] O. D. Chimitova,[f] Cheng-Peng Diao,[g] T. A. Gavrilova,[h] V. G. Kesler,[i] M. S. Molokeev,[j] A. S. Krylov,[k] B. G. Bazarov,[f] J. G. Bazarova[f] and Zheshuai Lin*[l]

Received 17th October 2014,
Accepted 13th November 2014

DOI: 10.1039/c4dt03203a

www.rsc.org/dalton

Microcrystals of orthorhombic rubidium samarium molybdate, β-RbSm$(MoO_4)_2$, have been fabricated by solid state synthesis at T = 450 °C, 70 h, and at T = 600 °C, 150 h. The crystal structure has been refined by the Rietveld method in space group *Pbcn* with cell parameters a = 5.0984(2), b = 18.9742(6) and c = 8.0449(3) Å (R_B = 1.72%). Thermal properties of β-RbSm$(MoO_4)_2$ were traced by DSC over the temperature range of T = 20–965 °C, and the earlier reported β ↔ α phase transition at T ~ 860–910 °C was not verified. The electronic structure of β-RbSm$(MoO_4)_2$ was studied by employing theoretical calculations and X-ray photoelectron spectroscopy. It has been established that the O 2p-like states contribute mainly to the upper part of the valence band and occupy the valence band maximum, whereas the Mo 4d-like states contribute mainly to the lower part of the valence band. Chemical bonding effects have been analysed from the element core level binding energy data. In addition, it was found that the luminescence spectrum of β-RbSm$(MoO_4)_2$ is rather peculiar among the Sm^{3+} containing materials. The optical refractive index dispersion in β-RbSm$(MoO_4)_2$ was also predicted by the first-principles calculations.

1. Introduction

Molybdate crystals possess interesting combinations of structural, chemical and spectroscopic properties that are promising for applications of the compounds in photochemistry, laser technology and functional electronics.[1–6] In oxide crystals, the Mo^{6+} ion can be coordinated by four or six oxygen ions, and the resulting molybdenum coordination polyhedra can be strongly distorted. These specific structural features generate a diverse crystal chemistry of complex molybdates and provide high feasibility for the incorporation of different doping metals, including rare-earth elements.[7–13] Several complex molybdates have been grown in the single crystal form, and basic physical parameters have been measured in detail.[14–20] However, only for a limited number of simple and complex Mo^{6+}-oxides have the electronic structures been studied by theoretical or experimental methods.[21–29]

The low-temperature modification β-RbSm$(MoO_4)_2$, space group *Pbcn*, was found in the quasi-binary system Rb_2MoO_4–$Sm_2(MoO_4)_3$ at Rb : Sm = 1 : 1, and it exists below the temperature T ~ 890–910 °C.[30,31] The synthesis route of the phase-pure β-RbSm$(MoO_4)_2$ was designed recently, and the crystal structure and atomic vibrational properties were determined using powder techniques.[32] However, the electronic structure properties of this compound remain unknown. On the one hand, X-ray photoelectron spectroscopy (XPS) measurements of Rb^+- and Sm^{3+}-containing crystals are very scarce in the literature, and the comparison of the ions' behavior in different compounds is topical. As it is known, the element core level binding energy (BE) is a parameter sensitive to chemical bond ionicity.[33–35] Thus, the measurement of the metal and oxygen core levels in β-RbSm$(MoO_4)_2$ can be used to analyze comparatively the metal–oxygen bonding characteristics by employing

[a]*Laboratory of Optical Materials and Structures, Institute of Semiconductor Physics, SB RAS, Novosibirsk 630090, Russia. E-mail: atuchin@isp.nsc.ru*
[b]*Functional Electronics Laboratory, Tomsk State University, Tomsk 634050, Russia*
[c]*Laboratory of Semiconductor and Dielectric Materials, Novosibirsk State University, Novosibirsk 630090, Russia*
[d]*Laboratory of Coherent Optics, Kirensky Institute of Physics, SB RAS, Akademgorodok, Krasnoyarsk 660036, Russia*
[e]*Siberian Federal University, Svobodnii 79, Krasnoyarsk 660041, Russia*
[f]*Laboratory of Oxide Systems, Baikal Institute of Nature Management, SB RAS, Ulan-Ude 670047, Russia*
[g]*General Research Institute for Nonferrous Metals, Beijing 100088, P. R. China*
[h]*Laboratory of Nanodiagnostics and Nanolithography, Institute of Semiconductor Physics, SB RAS, Novosibirsk 90, 630090, Russia*
[i]*Laboratory of Physical Bases of Integrated Microelectronics, Institute of Semiconductor Physics, SB RAS, Novosibirsk 90, 630090, Russia*
[j]*Laboratory of Crystal Physics, Kirensky Institute of Physics, SB RAS, Krasnoyarsk 660036, Russia*
[k]*Laboratory of Molecular Spectroscopy, Kirensky Institute of Physics, SB RAS, Krasnoyarsk 660036, Russia*
[l]*Technical Institute of Physics and Chemistry, Chinese Academy of Sciences, Beijing 100190, P. R. China. E-mail: zslin@mail.ipc.ac.cn*

†Electronic supplementary information (ESI) available. See DOI: 10.1039/c4dt03203a

the earlier proposed algorithm.[36–38] Meanwhile, accurate first-principles calculations on β-$RbSm(MoO_4)_2$ and their comparison with the XPS measurements are of great importance to deeply investigate the physical properties of the rare-earth element compounds. The present study, therefore, is aimed at the synthesis and detailed complementary evaluations of the electronic structure of binary orthorhombic β-$RbSm(MoO_4)_2$ by XPS and first-principles calculations. Structural, thermal, optical and spectroscopic parameters of the molybdate are also analyzed in detail.

2. Experimental methods

The polycrystalline β-$RbSm(MoO_4)_2$ sample was derived for the present experimental studies by solid state synthesis using a stoichiometric ratio mixture of analytically pure MoO_3 (99.9%), Rb_2CO_3 (99.99%), and Sm_2O_3 (>99.9%) as initial materials. The reagents were supplied by Novosibirsk rare metal plant (Russia). The MoO_3 oxide is volatile at comparatively high temperatures and, consequently, partial loss of this component during long duration synthesis may induce a deviation from the molybdate stoichiometry.[8,9,12,18,39] For this reason, a multistage method with step-by-step temperature increase was applied for the synthesis. The rubidium and samarium molybdates were prepared initially by a routine ceramic technique. Heat treatment of stoichiometric mixtures of the initial materials was started at T = 450 °C and followed by step-wise temperature increases up to T = 600 °C (Rb_2MoO_4) and 1073 °C ($Sm_2(MoO_4)_3$), respectively. Consequently, the Rb_2MoO_4 and $Sm_2(MoO_4)_3$ were ground and mixed in the stoichiometric composition $Rb_2MoO_4 : Sm_2(MoO_4)_3$ = 1 : 1. The powder mixture of the compounds was preheated at T = 450 °C for about 70 h and annealed at T = 600 °C for 150 h to yield the $RbSm(MoO_4)_2$ composition. After heat treatment, the powder sample was cooled to room temperature while remaining in the furnace. The phase purity of the intermediate simple molybdates and the final product were verified by powder X-ray dif-fraction (XRD) analysis using a D8 advance Bruker AXS diffractometer employing Cu Kα irradiation and a linear VANTEC detector. The step size of 2θ was 0.02°, and the counting time was 1 s per step. Micromorphology of the particles was observed by SEM using a LEO 1403 device.

The thermal behavior of the rubidium samarium molybdate was examined by differential scanning calorimetry (DSC) using a Netzsch STA 449 F1 Jupiter device over the temperature range 20–1200 °C. The β-$RbSm(MoO_4)_2$ powder was placed into a platinum crucible and heated up and cooled down under an argon atmosphere at the rate of 5 °C min^{-1}.

The electronic parameters of β-$RbSm(MoO_4)_2$ were observed with an XPS method using surface analysis center SSC (Riber). Nonmonochromatic Al Kα radiation (1486.6 eV) with a 300 W power source was used for the excitation of photoemission. The energy resolution of the instrument was chosen to be 0.7 eV, so as to have a sufficiently small broadening of natural core level lines at a reasonable signal-to-noise ratio. Under these conditions, the observed full width at half maximum (FWHM) of the Au $4f_{7/2}$ line was 1.31 eV. The binding energy (BE) scale was calibrated with reference to the Cu $3p_{3/2}$ (75.1 eV) and Cu $2p_{3/2}$ (932.7 eV) lines, assuring the accuracy of 0.1 eV in any peak energy position determination. The photoelectron energy drift due to charging effects was taken into account with reference to the position of the C 1s (284.6 eV) line generated by adventitious carbon present on the surface of the powder as inserted into the vacuum chamber. The chemical composition was determined using the detailed spectra of Rb 3d, Sm $3d_{5/2}$, Mo $3d_{5/2}$ and O 1s core levels and the known element sensitivity factors.[40]

Luminescence spectra of β-$RbSm(MoO_4)_2$ were measured using a LOMO DFS-24 double spectrometer equipped with a Hamamatsu photomultiplier. Spectral resolution was 3 cm^{-1}. A LaserCompact LCS-DTL-374QT DPSS laser generating up to 20 mW at 355 nm wavelength was used as the excitation source in these measurements.

3. Computational methods

The first-principles calculations for the β-$RbSm(MoO_4)_2$ crystal were performed by the plane-wave pseudopotential method[41] implemented in the CASTEP package[42] based on the density functional theory (DFT).[43] The structural parameters were determined in the present study. The ion–electron interactions were modeled by the optimized normal-conserving pseudopotentials[44,45] for all constituent elements, and the O $2s^2 2p^4$, Rb $4s^2 4p^6 5s^1$, Sm $5s^2 5p^6 4f^6 6s^2$, Mo $4d^5 5s^1$ electrons were treated as the valence electrons, respectively. It is well known that standard local density approximation (LDA) approaches have a major deficiency for studying systems containing transition metal or rare-earth metal ions with partially filled d (or f) shells. Thus, the LDA+U method,[46] in which the Hubbard U is applied on Sm (6.0 eV) and Mo (3.0 eV on 4d orbitals), was employed to perform the electronic structure calculations on β-$RbSm(MoO_4)_2$. Based on the calculated electronic band structure, the optical properties for β-$RbSm(MoO_4)_2$ were determined, and the dispersion of refractive index was predicted.

4. Results and discussion

After the high temperature synthesis, the final powder product was of white color with the light orange tint common for the Sm^{3+}-containing transparent oxides.[47–49] The recorded XRD pattern is shown in Fig. 1, and almost all the peaks were attributed to the β-$RbSm(MoO_4)_2$ molybdate.[32] Rietveld refinement was performed using the TOPAS 4.2 package.[50] The refinement was stable and gave low R-factors, as presented in Table 1. The atomic coordinates and chemical bond lengths in β-$RbSm(MoO_4)_2$ are shown in Tables 1S and 2S,† respectively. The higher precision structure determination was achieved due to wider 2θ range and higher accumulation time than those used

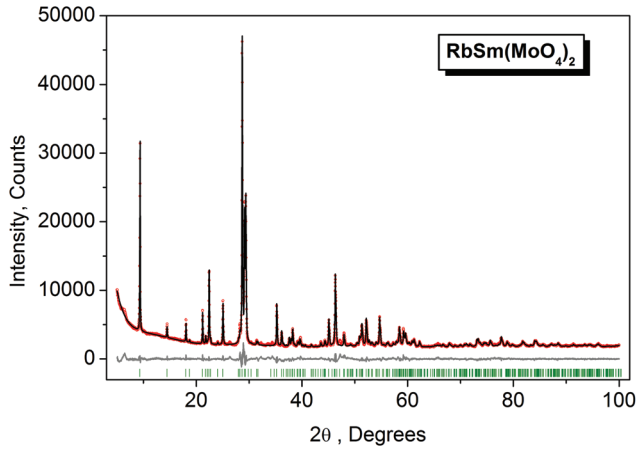

Fig. 1 Powder XRD pattern of β-RbSm$(MoO_4)_2$ used for Rietveld structure analysis.

Table 1 Main parameters of processing and refinement of the RbSm $(MoO_4)_2$ sample

Space group	*Pbcn*
a (Å)	5.0984(2)
b (Å)	18.9742(6)
c (Å)	8.0449(3)
V (Å^3)	778.24(5)
Z	8
2*θ*-interval, °	5–100
Number of reflections	405
Number of parameters of refinement	65
R_{wp} (%)	4.82
R_p (%)	3.36
R_{exp} (%)	1.90
χ^2	2.54
R_B (%)	1.72

in ref. 32. The obtained crystal structure of β-RbSm$(MoO_4)_2$ is shown in Fig. 2.[51]

The micromorphology of the final powder product is shown in Fig. 3. The observed microparticles are formed by agglomerated plate-like crystals with typical dimensions of ~2 μm and smoothed edges. Such a crystal habit appears to be governed by the layered structure common for the RbLn$(MoO_4)_2$-type molybdates.[6,32,39] During SEM pattern recording, the β-RbSm$(MoO_4)_2$ powder possessed drastic surface charging effects that confirmed high dielectric properties of the sample.

The DSC curve recorded from the β-RbSm$(MoO_4)_2$ powder sample is shown in Fig. 4. The endothermic signal at 965 °C was detected during the sample heating. During cooling, RbSm$(MoO_4)_2$ showed an exothermic effect confirming temperature of crystallization at 918 °C. The difference between the melting and crystallization temperatures seems to be due to a supercooling effect. It should be pointed out that the melting temperature of 965 °C measured in the present experiment is in good relation to the previously reported value of ~960 °C.[31] However, contrary to the earlier reports in the literature that mentioned the existence of the β ↔ α phase transition at T ~ 860–910 °C,[30,31] in our DSC measurements no signature was detected that may be attributed to the β ↔ α transition range

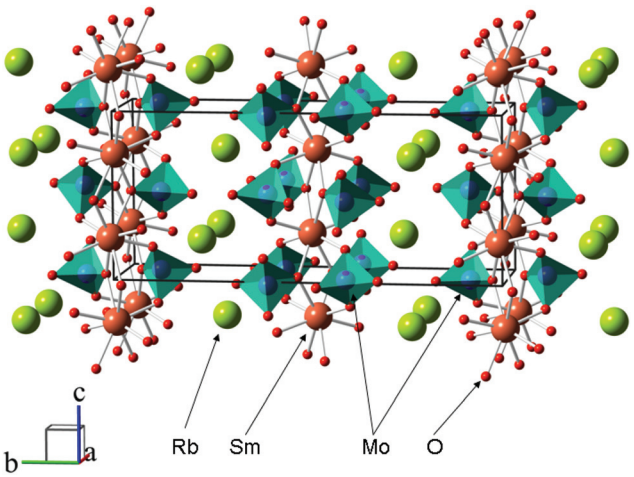

Fig. 2 Crystal structure of β-RbSm$(MoO_4)_2$, space group *Pbcn*. Lone atoms of samarium, molybdenum and oxygen are removed. Unit cell is outlined.

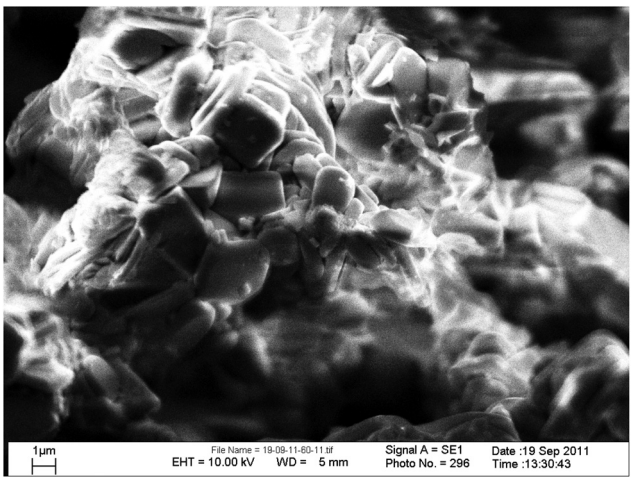

Fig. 3 SEM pattern of the β-RbSm$(MoO_4)_2$ microparticles.

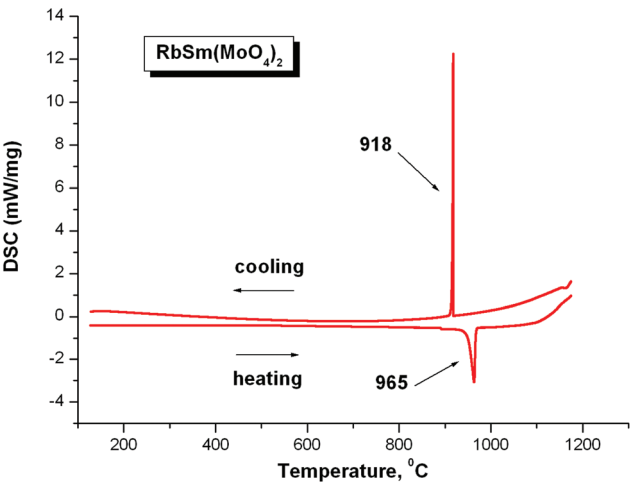

Fig. 4 DSC results obtained from β-RbSm$(MoO_4)_2$.

of $RbSm(MoO_4)_2$. Thus, the β-$RbSm(MoO_4)_2$ phase is stable at least down to room ambient temperature, and the previously reported phase transition could be attributed to insufficient purity of the reagents used. The phase transition absence over the range of T = 20–965 °C opens up the possibility of $RbSm(MoO_4)_2$ single crystal growth directly from the stoichiometric melt by an efficient Czochralski technique.

The survey photoemission spectrum of β-$RbSm(MoO_4)_2$ is shown in Fig. 5(a). All spectral features detected were successfully attributed to the constituent element core levels or Auger lines, except for a weak C 1s line superimposed on the Sm $4p_{1/2}$ line, as shown in Fig. 1S.† In Fig. 5(b)–(e), the representative element core levels Rb 3d, Rb 3p, Mo 3d, O 1s, and Sm 3d are shown. Additively, detailed spectra of a low-intensity Mo 3p doublet and Mo 4s, Mo 3s, Rb 3s and Sm 4s lines are shown in Fig. 2S–5S.† It should be noted that a weak intensity shoulder at the low-energy side of all the element peaks was detected, which seems to be due to the difference charging effect occasionally observed in dielectric powder samples.[52] For instance, the tail component of the Rb 3d peak can be found at a BE of 106.1 eV, as shown in Fig. 5(b). Meanwhile, Fig. 5(b) shows the complex structure of the Sm 4d band in β-$RbSm(MoO_4)_2$ in which several components can be revealed by a fitting analysis similar to earlier results obtained for several Sm^{3+}-containing oxides.[53–56] In Fig. 5(c) the pronounced superpositions of the Mo $3d_{3/2}$ and Rb $3p_{3/2}$, and the Rb $3p_{1/2}$ and Sm $4p_{3/2}$ lines are observed in β-$RbSm(MoO_4)_2$, and the respective BE values of the components were determined by a fitting analysis. The spectrum of the O 1s core level is shown in Fig. 5(d). The O 1s line is found to have the main component at 529.8 eV and two weak intensity components at 526.9 and 531.9 eV. The small peak at the higher BE of 531.9 eV

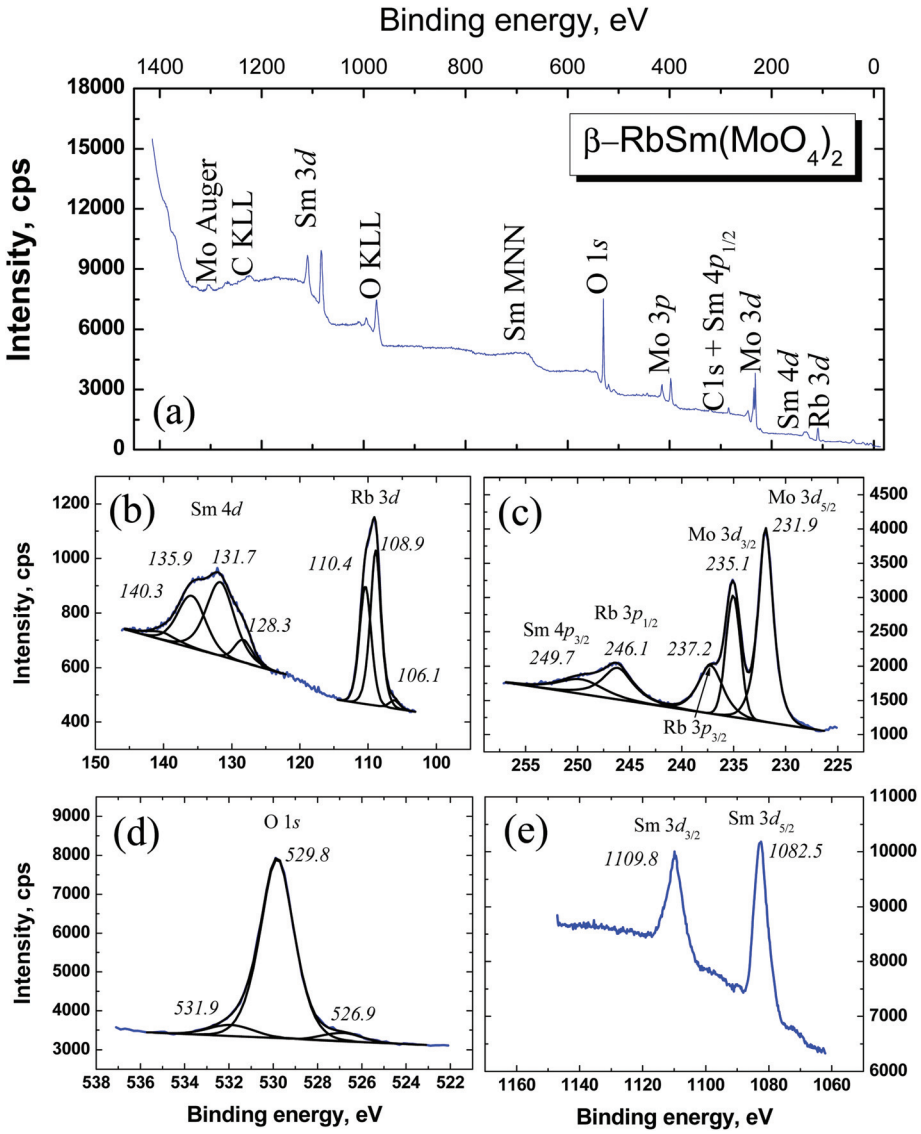

Fig. 5 (a) Survey XPS spectrum of the β-$RbSm(MoO_4)_2$ molybdate under consideration, and the detailed XPS spectrum of (b) the Rb 3d–Sm 4d window, (c) the Mo 3d–Sm $4p_{3/2}$ window, (d) the O 1s core level, and (e) the Sm 3d doublet.

may be due to adsorbed OH groups and the other two components seem to be related to oxygen states in the crystal bulk. In addition, the Sm 3d doublet is shown in Fig. 5(e). The doublet components are intense and have sharp maximums. It should be pointed out that the Sm 3d doublet shape measured in β-$RbSm(MoO_4)_2$ is very similar to that previously recorded from a nanocrystalline $SmAlO_3$ sample.[56]

The chemical composition was estimated by representative element peak areas and tabulated atomic sensitivity factors.[40] The relative element ratio for the powder sample is Rb : Sm : Mo : O = 0.10 : 0.07 : 0.19 : 0.64, which is reasonably consistent with the nominal composition of Rb : Sm : Mo : O = 0.08 : 0.08 : 0.17 : 0.67. The calculations were performed without carbon signal accounting. The Auger parameter determined for oxygen in β-$RbSm(MoO_4)_2$ is α_O = 1041.95 eV. The calculated Auger parameter of molybdenum for Mo $3d_{5/2}$ and Mo $M_{45}N_{23}V$ peaks is α_{Mo} = 413.9 eV. The Auger lines of all constituent elements are shown in Fig. 6S–9S.† The element core levels and Auger lines measured for β-$RbSm(MoO_4)_2$ are shown in Table 2.

In order to confirm the assignment of the respective orbitals observed in experiments, the first-principles electronic density of states (DOS) and partial DOS (PDOS) projected on the constituent atoms in $RbSm(MoO_4)_2$ were calculated, and their comparison to the experimental XPS spectrum is displayed in Fig. 6. It is clear that very good agreement between the experimental and calculated spectra is achieved if the energy zero point of the latter spectra shifts left about 3 eV, demonstrating the suitability of our computational method for β-$RbSm(MoO_4)_2$. In the PDOS, Mo 4p orbitals are not shown since they were not included in the electronic structure calculations. Both experimental and calculated results reveal that Rb 4s and 4p orbitals are much localized and have very weak chemical bonds with the other atoms. In comparison, Mo 4d and Sm 5f orbitals have quite large hybridization with O 2p states, indicating the relatively strong covalent bonds between

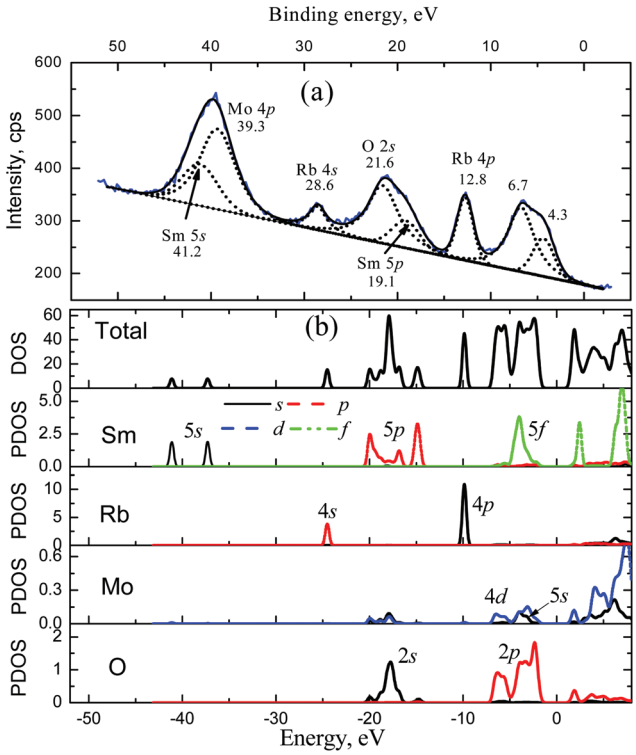

Fig. 6 Comparison of (a) experimental XPS spectrum and (b) *ab initio* electronic structures.

Table 2 Constituent element core levels and Auger lines in β-$RbSm(MoO_4)_2$

Core level (auger line)	Binding energy (eV)	Core level (auger line)	Binding energy (eV)
VB	4.3, 6.7		
Rb 4p	12/8	C 1s	Fixed at 284.6
Sm 5p	19.1	Rb 3s	320.8
O 2s	21.6	Sm 4s	348.7
Rb 4s	28.6	Mo $3p_{3/2}$	397.7
Mo 4p	39.3	Mo $3p_{1/2}$	415.1
Sm 5s	41.2	Mo 3s	508.9
Mo 4s	66.5	O 1s	529.8
Rb 3d	108.9, 110.4	Sm MNN	681.5, 703.6, 719.2
Sm 3d	128.3, 131.7, 135.9, 140.3	O KLL	974.5, 994.6
Mo $3d_{5/2}$	231.9	Sm $3d_{5/2}$	1082.5
Mo $3d_{3/2}$	235.1	Sm $3d_{3/2}$	1109.8
Rb $3p_{3/2}$	237.2	Mo MNV	1298.9, 1304.3
Rb $3p_{1/2}$	246.1	Rb Auger	~1368.5, ~1385.9
Sm $4p_{3/2}$	249.7		
Sm $4p_{1/2}$	284.4		

Mo–O and Sm–O. The peaks located at about 6.7 eV and 4.3 eV in the XPS spectrum were not explicitly assigned to the specific orbitals during the measurement, since they are composed of the combined contribution from O 2p, Sm 5f, and Mo 4d and 5s orbitals.

Chemical bonding in β-$RbSm(MoO_4)_2$ can be characterized by the BE of Rb $3d_{5/2}$, Sm $3d_{5/2}$, Mo $3d_{5/2}$ and O 1s lines. When rubidium, samarium and molybdenum interact with oxygen, valence electrons are transferred from metals to oxygens with variation of electrical screening of inner shells. As a result, BEs of inner electrons of metal ions increase with a synchronous decrease of BE of the O 1s level of oxygen ions. Combination of the three different metals with different ionicity in one ternary oxide, such as Rb, Sm and Mo in the case of β-$RbSm(MoO_4)_2$, generates small additive BE shifts because of specific redistribution of the electron density during atomic ordering and crystal lattice formation. For quantitative comparison of different oxides, it is suitable to use the difference between the BE of the selected metal and the BE of the O 1s core level.[36–38,57–62] This method avoids drastic scatter in BE values due to strong surface charging of the dielectric oxide surface resulting from the photoelectron emission under X-ray illumination, and gives a robust quantitative criterion for the comparison of electronic parameters measured in different studies and using different XPS spectrometers. For the β-$RbSm(MoO_4)_2$ molybdate, the BE differences Δ_{Rb} = (BE O 1s–BE Rb $3d_{5/2}$), Δ_{Sm} = (BE O 1s–BE Sm $3d_{5/2}$) and Δ_{Mo} = (BE O 1s–BE Mo $3d_{5/2}$) are suitable.

Up to now, the Rb 3d doublet components together with the O 1s core level have been defined only in Rb_2CO_3, $RbHCO_3$, Rb_2SO_4 and $RbTiOPO_4$.[62–64] The collection of the XPS results and related structural information are shown in Table 3. It should be noted that the crystal structure of $RbHCO_3$ remains unknown. Evidently, the collection of Rb-containing crystals is very limited, which excludes a consideration of the relationship between Δ_{Rb} and mean chemical bond length L(Rb–O). However, it can be concluded that Δ_{Rb}(β-RbSm$(MoO_4)_2$) hits into the range of Δ_{Rb} = 420.5–421.5 eV found for the Rb-containing oxides.

To the best of our knowledge, the Sm 3d doublet components together with the O 1s core level have been determined only in six oxide crystals.[55,56,68–70] The collection of the XPS results and related structural information are shown in Table 4. Here, on the determination of the mean bond length L(Sm–O), the Sm–O bonds were accounted whose length is below the limit of 250 pm. The diagram of Δ_{Sm}–L(Sm–O) is shown in Fig. 7(a). There is no clear trend in the L(Sm–O) variation, and the points form a cluster. However, this may be because only a very limited number of Sm-containing oxide crystals have been measured by XPS up to now, and some trend could be revealed on further accumulation of experimental data. The value of Δ_{Sm}(β-RbSm$(MoO_4)_2$) = −552.7 eV is at the upper boundary of the cluster, and this indicates a relatively low mean ionicity of the Sm–O bonds in β-RbSm$(MoO_4)_2$.

It is particularly interesting to consider the Mo–O chemical bonding in molybdate compounds using the Δ_{Mo} parameter as an indicator of mean bond ionicity. The mean chemical bond length L(Mo–O) calculated from the available crystal structure

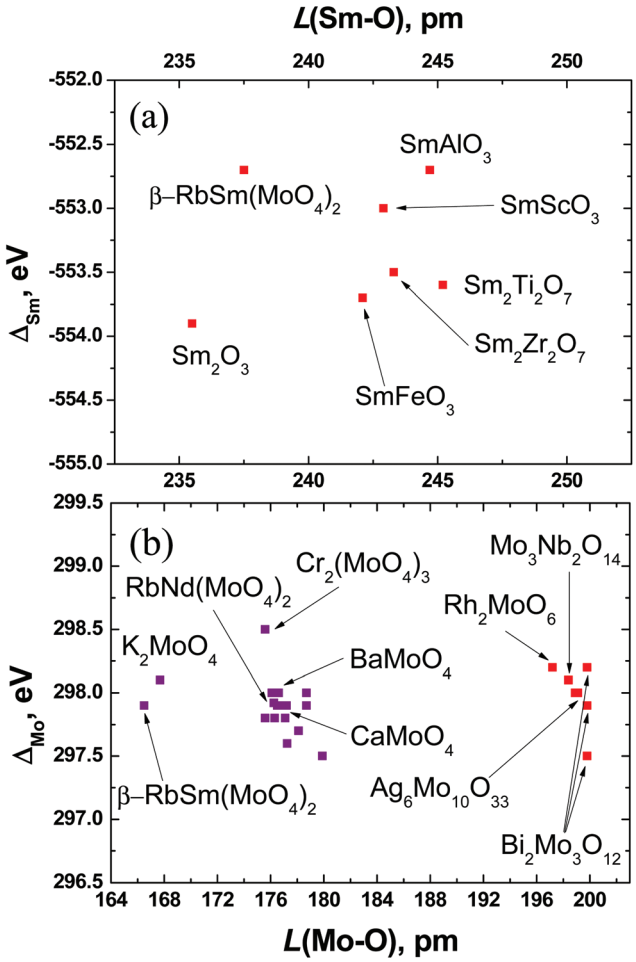

Fig. 7 Dependence of (a) Δ_{Sm} on L(Sm–O) in oxide crystals, and (b) Δ_{Mo} on L(Mo–O) in molybdates.

Table 3 Core level and structural parameters of Rb-containing oxide crystals

Crystal	Rb $3d_{5/2}$ (eV)	O 1s (eV)	Δ_{Rb} (eV)	Ref.	L(Rb–O) (pm)	Ref.
Rb_2CO_3	109.4	530.1	420.7	62	294.0	65
$RbHCO_3$	109.2	530.7	421.5	62	—	—
Rb_2SO_4	109.8	531.3	421.5	63	306.2	66
$RbTiOPO_4$	109.9	530.4	420.5	64	299.3	67
β-RbSm$(MoO_4)_2$	108.9	529.8	420.9	Present study	296.2	Present study

Table 4 Core level and structural parameters of Sm-containing oxide crystals

Crystal	Sm $3d_{5/2}$ (eV)	O 1s (eV)	Δ_{Sm} (eV)	Ref.	L(Sm–O) (pm)	Ref.
Sm_2O_3	1083.1	529.2	−553.9	55	235.5	71
$SmAlO_3$	1082.5	529.8	−552.7	56	244.7	72
$SmFeO_3$	1082.6	528.9	−553.7	68	242.1	73
$SmScO_3$	1082.9	529.9	−553.0	70	242.9	74
$Sm_2Ti_2O_7$	1082.8	529.2	−553.6	69	245.2	75
$Sm_2Zr_2O_7$	1082.5	529.0	−553.5	69	243.3	76
β-RbSm$(MoO_4)_2$	1082.5	529.8	−552.7	Present study	237.5	Present study

data is taken as a structure related parameter. So, the collection of electronic and structural parameters presently available for molybdates is depicted in Table 5. The diagram with these molybdates is shown in Fig. 7(b). The crystals show the Δ_{Mo} dominantly in the range 297.6–298.2 eV with several exceptions. The molybdates with tetrahedral MoO_4 lie in the range of L(Mo–O) = 166–180 pm, and β-RbSm$(MoO_4)_2$ relates to this group. The molybdates with octahedral coordination of Mo^{6+} ions possess the range of L(Mo–O) = 196–200 pm. However, both molybdate groups, with tetrahedral MoO_4 and octahedral MoO_6, show nearly the same level of the Δ_{Mo} parameter. Generally, this indicates that there is no noticeable dependence of (Mo–O) bond ionicity on the coordination type of Mo^{6+} ions by oxygens. It should be noted that previously the same result was found for (W–O) bonding in tungstates.[117] Thus, it can be concluded that the behavior of (Mo–O) and (W–O) bonds is very similar. In contrast, the electronic parameters of (Mo–O) bonds in oxyfluoromolybdates are drastically different from those in molybdates.[118] It is interesting to compare the Δ_{Mo} parameters obtained for β-RbSm$(MoO_4)_2$ and β-RbNd$(MoO_4)_2$ from the same crystal family.[116] The XPS experiments were performed using different spectrometers and the measured BE

Table 5 Core level and structural parameters of molybdate crystals

Crystal	Mo $3d_{5/2}$ (eV)	O 1s (eV)	Δ_{Mo} (eV)	Ref.	L(Mo–O) (pm)	Ref.
Na_2MoO_4	232.2	530.1	297.9	77	178.7	94
	232.2	530.2	298.0	78		
K_2MoO_4	232.3	530.4	298.1	78	167.7	95
$CuMoO_4$	232.9	530.8	297.9	79	177.2	96
$Cu_3Mo_2O_9$	233.0	530.8	297.8	79	176.3	97
$Cu_{3.85}Mo_3O_{12}$	232.7	530.7	298.0	79	175.6	98
$MgMoO_4$	233.2	531.1	297.9	78	176.5	99
$MnMoO_4$	233.0	531.0	298.0	78	176.1	100
α-$FeMoO_4$	232.5	530.8	298.3	80	182.6	101
β-$FeMoO_4$	231.7	530.3	298.6	81	176.4	101
$CoMoO_4$	231.1	529.1	298.0	82	182.7	102
	232.2	530.5	298.3	83		
	232.9	531.3	298.3	78		
$CaMoO_4$	233.0	530.8	297.8	78	177.1	103
	232.6	530.5	297.9	84		
$SrMoO_4$	232.9	530.8	297.9	78	177.0	104
$BaMoO_4$	232.7	530.7	298.0	78	176.6	105
	232.3	530.3	298.0	85		
$Al_2(MoO_4)_3$	233.5	531.5	298.0	78	176.1	106
$Cr_2(MoO_4)_3$	232.8	531.3	298.5	78	175.6	107
Bi_2MoO_6	233.0	530.6	297.6	86	177.3	108
	232.5	530.3	297.8	87		
$Bi_2Mo_2O_9$	233.0	530.8	297.8	86	175.6	109
Dy_2MoO_6	233.0	530.5	297.5	78	179.9	110
$Li_2Ni_2(MoO_4)_3$	232.8	530.9	298.1	88	177.6	111
$Li_3V(MoO_4)_3$	232.7	531.0	298.3	89	177.0	89
$Ag_6Mo_{10}O_{33}$	232.0	530.0	298.0	90	198.9	112
$Mo_3Nb_2O_{14}$	232.8	530.9	298.1	91	198.4	91
Rh_2MoO_6	232.0	530.2	298.2	92	197.2	113
α-$Bi_2Mo_3O_{12}$	233.2	530.7	297.5	86	199.8	114
	232.9	531.1	298.2	78		
	232.5	530.4	297.9	87		
Sr_2FeMoO_6	232.0	529.2	297.2	93	197.4	115
β-$RbNd(MoO_4)_2$	232.19	530.11	297.92	116	176.25	39
β-$RbSm(MoO_4)_2$	231.9	529.8	297.9	Present study	166.5	Present study

(O 1s) and BE (Mo $3d_{5/2}$) are noticeably different. Nevertheless, the Δ_{Mo} values are practically the same in both molybdates. This fact once again verifies the robustness of BE difference to the XPS spectrometer calibration difference.

Usually, the optical properties are very sensitive to the electronic structure in a crystal. Fig. 8 shows the first-principles refractive index dispersion in β-$RbSm(MoO_4)_2$ for the wavelength λ ranging from 400 nm to 2000 nm. Interestingly, β-$RbSm(MoO_4)_2$ exhibits an optical positive uniaxial behavior with $n_x > n_y \sim n_z$ for $\lambda < 450$ nm, whereas it manifests a negative uniaxial behavior with $n_x \sim n_y > n_z$ for $\lambda > 800$ nm (here $x \leftrightarrow a$, $y \leftrightarrow b$ and $z \leftrightarrow c$). In the major part of the visible region (400 nm $< \lambda <$ 800 nm), this crystal exhibits an optical biaxial character. The unusual modification of optical properties actually reflects the changed response of electronic clouds (or chemical bonds) to the varied incident light frequency in β-$RbSm(MoO_4)_2$: in the lower photon energy range the chemical bonds are isotropic in the y–z plane (or b–c plane), while in the higher photon energy range they are isotropic in the x–y plane (or a–b plane). A detailed mechanism analysis will have to wait for future studies when β-$RbSm(MoO_4)_2$ crystals with large size and high quality are obtained.

The room temperature luminescence spectrum of β-$RbSm(MoO_4)_2$ under 355 nm excitation is shown in Fig. 9. The most probable excitation channel for the wavelength used is the transition from the ground state ($^6H_{5/2}$) to the excited $^4H_{7/2}$ state.[119] The luminescence spectrum of β-$RbSm(MoO_4)_2$ is rather peculiar among Sm^{3+}-containing materials. It is dominated by the band peaking at 574 nm (17 420 cm^{-1}). This line

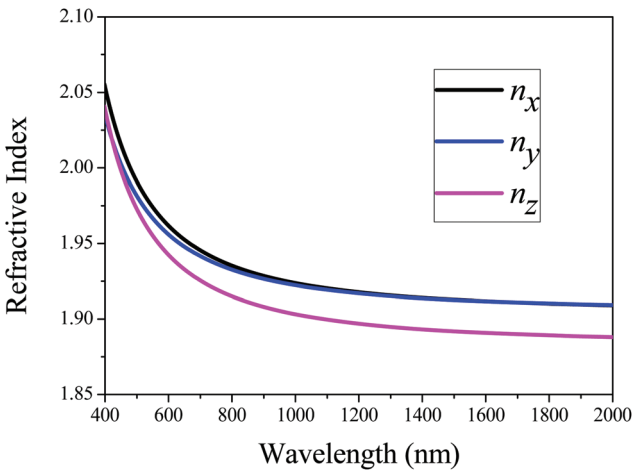

Fig. 8 First-principles refractive index dispersion over the wavelength range from 400 to 2000 nm in β-$RbSm(MoO_4)_2$.

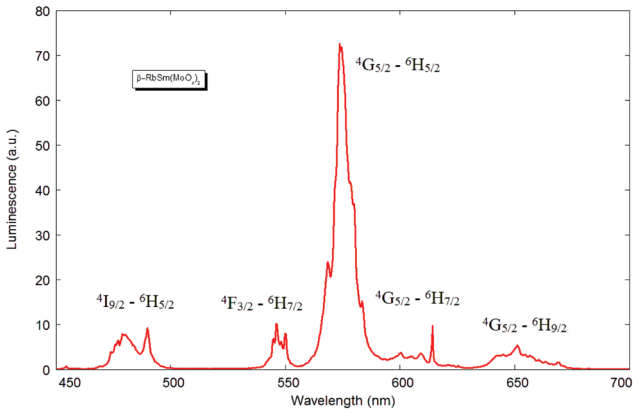

Fig. 9 Room temperature luminescence spectrum of β-RbSm$(MoO_4)_2$ excited at 355 nm.

can be observed, *e.g.*, in a 77 K samarium-doped yttrium gallium garnet spectrum,[120] where the dominating line is positioned at 569.5 nm. The same line is observed in the room temperature spectrum of $LaMgB_5O_{10}$–Sm^{3+} ref. 121 where it was ascribed to the transition from $^4G_{5/2}$ to the upper sublevel of the $^6H_{5/2}$ ground state. The dominating line in the latter material is at 596 nm, being due to the transition from $^4G_{5/2}$ to the lowest sublevel of $^6H_{7/2}$. The local symmetry of the Sm^{3+} ion in β-RbSm$(MoO_4)_2$ is C_2, and its environment is a square antiprism in the first approximation. In fact, a square antiprism is the limiting case of parity-breaking distortion from a cubic environment; this distortion is typical for garnets. The square antiprism in β-RbSm$(MoO_4)_2$ is additionally distorted, resulting in the scatter of Sm–O bond lengths within the 2.335–2.762 Å range. This distortion of the antiprism leads to lower symmetry of the Sm ion in β-RbSm$(MoO_4)_2$ than that in garnets (D_2). It is natural to ascribe the peculiarities of Sm^{3+} luminescence to the specific environment described above. In addition to three commonly observed luminescent bands of Sm^{3+} ($^4G_{5/2}$–$^6H_{9/2}$, $^4G_{5/2}$–$^6H_{7/2}$ and $^4G_{5/2}$–$^6H_{5/2}$), we observed the rarely observed $^4F_{3/2}$–$^6H_{7/2}$ and very rarely observed $^4I_{9/2}$–$^6H_{5/2}$ transitions. The intensity of the $^4I_{9/2}$–$^6H_{5/2}$ transition is even higher than the intensity of the hypersensitive $^4G_{5/2}$–$^6H_{9/2}$ transition. The observation of luminescence from $^4I_{9/2}$ is evidence of rather low radiativeless relaxation from this level in the structure of β-RbSm$(MoO_4)_2$.

5. Conclusions

High-quality β-RbSm$(MoO_4)_2$ molybdate has been obtained using a solid state synthesis method, and its crystal structure has been refined. The differential scanning calorimetry measurement reveals that, contrary to previous studies, this crystal does not exhibit the β ↔ α phase transition at $T \sim$ 860–910 °C. Moreover, the electronic structure of the β-RbSm$(MoO_4)_2$ molybdate has now been studied by X-ray photoelectron spectroscopy (XPS) and theoretical methods for the first time. The chemical bond analysis performed for β-RbSm$(MoO_4)_2$ in comparison with many other molybdates using the BE difference parameter Δ_{Mo} = (BE O 1s–BE Mo $3d_{5/2}$) obtained by the XPS measurements indicates the mean Mo–O bond ionicity independence on the Mo^{6+} ion coordination in oxides. Thus, it can be concluded that the behavior of (Mo–O) and (W–O) bonds in oxide crystals is very similar and different from that of (Ti–O) and (Nb–O) bonds.

Very good agreement between the experimental and calculated band spectra of β-RbSm$(MoO_4)_2$ has been achieved in the present study, demonstrating the suitability of our computational method for complex rare-earth bearing oxide crystals. Both experimental and calculated results reveal that Rb 4s and 4p orbitals are much localized, and the Rb^+ ions have very weak chemical bonds with the other atoms. However, the Mo 4d and Sm 5f orbitals have quite large hybridization with O 2p states, indicating that the Mo–O and Sm–O covalent bonds are relatively strong. The peaks located at about 6.7 eV and 4.3 eV in the XPS spectrum are identified to be composed of the combined contribution from O 2p, Sm 5f, and Mo 4d and 5s orbitals. The first-principles refractive index dispersion calculations reveal that the varied response of chemical bonds to the different incident light frequency results in the unusual modification in optical characteristics of β-RbSm$(MoO_4)_2$ from the visible to near-infrared spectral regions. The luminescence spectrum of β-RbSm$(MoO_4)_2$ is rather peculiar among Sm^{3+}-containing materials. It is governed by C_2 local symmetry of the samarium ion and is dominated by the band peaking at 574 nm ($^4G_{5/2}$ to $^6H_{5/2}$, 17 420 cm^{-1}).

As is well known, the band structure of Ln-bearing oxides is very dependent on the energy position of the Ln 5f orbitals in the valence band, and this feature is also observed in β-RbSm$(MoO_4)_2$. The ALn$(MoO_4)_2$ family of molybdates (A = alkaline cations) contains many members, so the present studies in β-RbSm$(MoO_4)_2$ can be selected as a suitable proving ground for the exploration of related electronic and spectroscopic effects in molybdates due to alkaline and rare-earth (Ln) element substitution.

Acknowledgements

VVA and ASA gratefully acknowledge the Ministry of Education and Science of the Russian Federation for financial support. ZL acknowledges the support by National Natural Science Foundation of China (11174297 and 11474292), the National Basic Research Project of China (2011CB922204), and Foundation of the Director of Technical Institute of Physics and Chemistry, CAS. The work was partially supported by RAS Project 24-29 and RFBR Grant 13-02-00825.

References

1 P. V. Klevtsov and R. F. Klevtsova, *J. Struct. Chem.*, 1977, **18**(3), 419.

2 T. T. Basiev, A. A. Sobol, Yu. K. Voronko and P. G. Zverev, *Opt. Mater.*, 2000, **15**, 205.
3 F. E. Osterloh, *Chem. Mater.*, 2008, **20**, 35.
4 A. Kudo and Y. Miseki, *Chem. Soc. Rev.*, 2009, **38**, 253.
5 M. Maczka, A. G. Souza Filho, W. Paraguassu, P. T. C. Freire, J. Mendes Filho and J. Hanuza, *Prog. Mater. Sci.*, 2012, **57**, 1335.
6 O. D. Chimitova, V. V. Atuchin, B. G. Bazarov, M. S. Molokeev and Z. G. Bazarova, *Proc. SPIE*, 2013, **8771**, 87711A.
7 L. Macalik, *Alloys Compd.*, 2002, **341**, 226.
8 B. G. Bazarov, R. F. Klevtsova, O. D. Chimitova, L. A. Glinskaya, K. N. Fedorov, Yu. L. Tushinova and Zh. G. Bazarova, *Russ. J. Inorg. Chem.*, 2006, **51**(5), 800.
9 V. G. Grossman, B. G. Bazarov, R. F. Klevtsova, S. F. Solodovnikov, L. A. Glinskaya, K. N. Fedorov and Z. G. Bazarova, *Russ. J. Inorg. Chem.*, 2008, **53**(10), 1660.
10 S. L. Chang, *Mater. Res. Bull.*, 2012, **47**, 4220.
11 Y. Li, G. F. Wang, K. Pan, W. Zhou, C. Wang, N. Y. Fan, Y. J. Chen, Q. M. Feng and B. B. Zhao, *CrystEngComm*, 2012, **14**, 5015.
12 A. E. Sarapulova, B. Bazarov, T. Namsaraeva, S. Dorzhieva, J. Bazarova, V. Grossman, A. A. Bush, I. Antonyshyn, M. Schmidt, A. M. T. Bell, M. Knapp, H. Ehrenberg, J. Eckert and D. Mikhailova, *J. Phys. Chem. C*, 2014, **118**, 1763.
13 P. L. Shi, Z. G. Xia, M. S. Molokeev and V. V. Atuchin, *Dalton Trans.*, 2014, **43**, 9669.
14 A. A. Kaminskii, A. V. Butashin, H.-J. Eichler, D. Grebe, R. Macdonald, K. Ueda, H. Nishioka, W. Odajima, M. Tateno, J. Song, M. Musha, S. N. Bagaev and A. A. Pavlyuk, *Opt. Mater.*, 1997, **7**, 59.
15 C. Cascales, A. Méndez Blas, M. Rico, V. Volkov and C. Zaldo, *Opt. Mater.*, 2005, **27**, 1672.
16 C. V. Ramana, V. V. Atuchin, I. B. Troitskaia, S. A. Gromilov, V. G. Kostrovsky and G. B. Saupe, *Solid State Commun.*, 2009, **149**, 6.
17 J. J. Zhang, Z. H. Zhang, Y. X. Sun, C. Q. Zhang and X. T. Tao, *CrystEngComm*, 2011, **13**, 6985.
18 V. V. Atuchin, T. A. Gavrilova, T. I. Grigorieva, N. V. Kuratieva, K. A. Okotrub, N. V. Pervukhina and N. V. Surovtsev, *J. Cryst. Growth*, 2011, **318**, 987.
19 J. J. Zhang, Z. L. Gao, X. Yin, Z. H. Zhang, Y. X. Sun and X. T. Tao, *Appl. Phys. Lett.*, 2012, **101**, 062901.
20 V. A. Trifonov, A. A. Pavlyuk, K. N. Gorbachenya, A. S. Yasyukevich and N. V. Kuleshov, *Inorg. Mater.*, 2013, **49**(5), 517.
21 Y. Abrahams, N. A. W. Holzwarth and R. T. Williams, *Phys. Rev. B: Condens. Matter*, 2000, **62**(3), 1733.
22 J. A. Rodriguez, J. C. Hanson, S. Chaturvedi, A. Maiti and J. L. Brito, *J. Phys. Chem. B*, 2000, **104**(34), 8145.
23 M. Fujita, M. Itoh, S. Takagi, T. Shimizu and N. Fujita, *Phys. Status Solidi B*, 2006, **243**(8), 1898.
24 S. F. Matar, A. Largeteau and G. Demazeau, *Solid State Sci.*, 2010, **12**(10), 1779.
25 H. Zhao, X. F. Guo and Q. R. Zhang, *Chin. J. Physiol.*, 2010, **48**(5), 662.
26 C. L. Hu and J. G. Mao, *J. Phys.: Condens. Matter*, 2010, **22**, 155801.
27 L. S. Cavalcante, E. Moraes, M. A. P. Almeida, C. J. Dalmaschio, N. C. Batista, J. A. Varela, E. Longo, M. S. Li, J. Andses and A. Beltran, *Polyhedron*, 2013, **54**, 13.
28 S. G. Zhao, X. X. Jiang, R. He, S. Q. Zhang, Z. H. Sun, J. H. Luo, Z. S. Lin and M. C. Hing, *J. Mater. Chem.*, 2013, **C1**(16), 2906.
29 Y. Hizhnyi, S. Nedilko, V. Chornii, T. Nikolaenko, I. Zatovsky, K. Terebilenko and R. Boiko, *Solid State Phenomena*, 2013, **200**, 114.
30 V. K. Rybakov, V. K. Trunov and V. I. Spitsyn, *Dokl. Akad. Nauk UzSSR*, 1970, **192**(2), 369.
31 T. P. Rybakova and V. K. Trunov, *J. Inorg. Chem.*, 1973, **18**(9), 2583.
32 V. V. Atuchin, O. D. Chimitova, S. V. Adichtchev, B. G. Bazarov, T. A. Gavrilova, M. S. Molokeev, N. V. Surovtsev and Zh. G. Bazarova, *Mater. Lett.*, 2013, **106**, 26–29.
33 V. I. Nefedov, N. P. Sergushin and Ja. V. Salyn, *J. Electron Spectrosc. Relat. Phenom.*, 1976, **8**, 83.
34 V. Dimitrov, T. Komatsu and R. Sato, *J. Ceram. Soc. Jpn.*, 1999, **107**(1), 21.
35 T. L. Barr, *Crit. Rev. Anal. Chem.*, 2012, **22**(3–4), 229.
36 V. V. Atuchin, V. G. Kesler, N. V. Pervukhina and Z. M. Zhang, *J. Electron Spectrosc. Relat. Phenom.*, 2006, **152**, 18–24.
37 V. V. Atuchin, V. G. Kesler and N. V. Pervukhina, *Surf. Rev. Lett.*, 2008, **15**(4), 391.
38 V. V. Atuchin, L. I. Isaenko, V. G. Kesler, L. Kang, Z. S. Lin, M. S. Molokeev, A. P. Yelisseyev and S. A. Zhurkov, *J. Phys. Chem. C*, 2013, **117**(14), 7269.
39 V. V. Atuchin, O. D. Chimitova, T. A. Gavrilova, M. S. Molokeev, S.-J. Kim, N. V. Surovtsev and B. G. Bazarov, *J. Cryst. Growth*, 2011, **318**, 683.
40 *Handbook of X-ray Photoelectron Spectroscopy*, ed. C. D. Wagner, W. M. Riggs, L. E. Davis, J. F. Moulder and G. E. Muilenberg, Perkin-Elmer Corp., Phys. Elect. Div., Minesota, 1979.
41 M. C. Payne, M. P. Teter, D. C. Allan, T. A. Arias and J. D. Joannopoulos, *Rev. Mod. Phys.*, 1992, **64**, 1045.
42 S. J. Clark, M. D. Segall, C. J. Pickard, P. J. Hasnip, M. J. Probert, K. Refson and M. C. Payne, *Z. Kristallogr.*, 2005, **220**, 567.
43 W. Kohn and L. J. Sham, *Phys. Rev. A*, 1965, **140**, 113.
44 A. M. Rappe, K. M. Rabe, E. Kaxiras and J. D. Joannopoulos, *Phys. Rev.*, 1990, **B41**, 1227.
45 J. S. Lin, A. Qtseish, M. C. Payne and V. Heine, *Phys. Rev.*, 1993, **B47**, 4174.
46 V. I. Anisimov, F. Aryasetiawan and A. I. Lichtenstein, *J. Phys.: Condens. Matter*, 1997, **9**, 767.
47 T. N. Khamaganova, N. M. Khrushcheva and Z. G. Bazarova, *Russ. J. Inorg. Chem.*, 1999, **44**(10), 1542.

48 Z. G. Bazarova, Y. L. Tushinova, B. G. Bazarov, R. F. Klevtsova, S. F. Solodovnikov, N. A. Pyl'neva, A. M. Yurkin and K. N. Fedorov, *Russ. J. Inorg. Chem.*, 2001, **46**(1), 135.
49 Z. G. Bazarova, E. Y. Badmaeva, S. F. Solodovnikov, Y. L. Tushinova, B. G. Bazarov and E. S. Zolotova, *Russ. J. Inorg. Chem.*, 2004, **49**(2), 284.
50 *Bruker AXS TOPAS V4: General profile and structure analysis software for powder diffraction data. – User's Manual*, Bruker AXS, Karlsruhe, Germany, 2008.
51 T. C. Ozawa and S. J. Kang, *J. Appl. Crystallogr.*, 2004, **37**, 679.
52 V. V. Atuchin, O. A. Alekseeva, V. G. Kesler, L. D. Pokrovsky, N. I. Sorokina and V. I. Voronkova, *J. Solid State Chem.*, 2006, **179**(8), 2349.
53 D. F. Mullica, C. K. C. Lok, H. O. Perkins, G. A. Benesh and V. Young, *J. Electron Spectrosc. Relat. Phenom.*, 1995, **71**, 1.
54 Yu. A. Teterin, T. N. Bondarenko, A. Yu. Teterin, A. M. Lebedev and I. O. Utkin, *Radiochemistry*, 1998, **40**(2), 107.
55 Yu. A. Teterin and A. Yu. Teterin, *Russ. Chem. Rev.*, 2002, **71**(5), 347.
56 D. Petrov, B. Angelov and V. Lovchinov, *J. Rare Earths*, 2010, **28**(4), 602.
57 Y. Fukuda, M. Nagoshi, T. Suzuki, Y. Namba, Y. Syono and M. Tachiki, *Phys. Rev. B: Condens. Matter*, 1989, **39**(16), 11494.
58 M. J. Guinet, J. P. Crocombette and M. Gautier-Soyer, *Phys. Rev. B: Condens. Matter*, 1989, **63**, 125117.
59 V. V. Atuchin, I. E. Kalabin, V. G. Kesler and N. V. Pervukhina, *J. Electron Spectrosc. Relat. Phenom.*, 2005, **142**, 129.
60 V. A. Shvets, V. Sh. Aliev, D. V. Gritsenko, S. S. Shaimeev, E. V. Fedosenko, S. V. Rykhlitski, V. V. Atuchin, V. A. Gritsenko, V. M. Tapilin and H. Wong, *J. Non-Cryst. Solids*, 2008, **354**, 3025.
61 T Mori, K Kajihara, K Kanamura, Y Toda, H Hiramatsu and H Hosono, *J. Am. Chem. Soc.*, 2013, **135**(35), 13080.
62 A. V. Shchukarev and D. V. Korolkov, *Cent. Eur. J. Chem.*, 2004, **2**(2), 347.
63 M. Wahlqvist and A. Shchukarev, *J. Electron Spectrosc. Relat. Phenom.*, 2007, **156**, 310.
64 V. V. Atuchin, V. G. Kesler, G. Meng and Z. S. Lin, *J. Phys.: Condens. Matter*, 2012, **24**, 405503.
65 H. Ehrhardt, H. Schweer and H. Seidel, *Z. Anorg. Allg. Chem.*, 1980, **462**, 185.
66 H. J. Weber, M. Schulz, S. Schulz, J. Granzin and H. Siegert, *J. Phys.: Condens. Matter*, 1989, **1**(44), 8543.
67 P. A. Thomas, S. C. Mayo and B. E. Watts, *Acta Crystallogr., Sect. B: Struct. Sci.*, 1992, **B48**, 401.
68 H. Aono, M. Sato, E. Traversa, M. Sakamoto and Y. Sadaoka, *J. Am. Ceram. Soc.*, 2001, **84**(2), 341.
69 J. M. Sohn, M. R. Kim and S. I. Woo, *Catal. Today*, 2003, **83**, 289.
70 C. Derks, *Characterization of $RScO_3$, $LuFe_2O_4$ and $M_{72}Fe_{30}$ based molecules by X-ray spectroscopic techniques*, Dissertation, Univ. Osnabrück, 2012.
71 A. Bartos, K. P. Lieb, M. Uhrmacher and D. Wiarda, *Acta Crystallogr., Sect. B: Struct. Sci.*, 1993, **49**, 165.
72 M. Marezio, P. D. Dernier and J. P. Remeika, *J. Solid State Chem.*, 1972, **4**, 11.
73 E. N. Maslen, V. A. Strel'tsov and N. Ishizawa, *Acta Crystallogr., Sect. B: Struct. Sci.*, 1996, **52**, 406.
74 R. P. Liferovich and R. H. Mitchell, *J. Solid State Chem.*, 2004, **177**, 2188.
75 O. Knop, F. Brisse, L. Castelliz and P. V. Thermoanalytic, *Can. J. Chem.*, 1969, **47**, 971.
76 F. N. Sayed, V. Grover, K. Bhattacharyya, D. Jain, A. Arya, C. S. G. Pillai and A. K. Tyagi, *Inorg. Chem.*, 2011, **50**(6), 2354.
77 S. F. Ho, S. Contarini and J. W. Rabalais, *Chem. Phys. Lett.*, 1987, **133**(2), 171.
78 V. I. Nefedov, *X-ray photoelectron spectroscopy of chemical compounds: Handbook*, Khimia, Moscow, 1984.
79 J. Huber, T. Machej, L. Ungier and J. Ziółkowski, *J. Solid State Chem.*, 1978, **25**, 207.
80 T. S. Sampathkumar, R. M. Mallya and M. S. Hegde, *Bull. Mater. Sci.*, 1985, **7**(5), 465.
81 Z. Y. Zhang, C. G. Hu, M. Hashim, P. Chen, Y. Q. Xiong and C. L. Zhang, *Mater. Sci. Eng., B*, 2011, **176**, 756.
82 P. Gajardo, D. Pirotte, C. Defosse, P. Grange and B. Delmon, *J. Electron Spectrosc. Relat. Phenom.*, 1979, **17**, 121.
83 N. S. McIntyre, D. D. Johnston, L. L. Coastworth, R. D. Davidson and J. R. Brown, *Surf. Interface Anal.*, 1990, **15**, 265.
84 H. N. Im, M. B. Choi, S. Y. Jeon and S. J. Song, *Ceram. Int.*, 2011, **37**, 49.
85 C. T. Xia and V. M. Fuenzalida, *J. Eur. Ceram. Soc.*, 2003, **23**, 519.
86 D. A. G. van Oeffelen, J. H. C. van Hooff and G. C. A. Schutt, *J. Catal.*, 1985, **95**, 84.
87 K. Uchida and A. Ayame, *Surf. Sci.*, 1996, **357–358**, 170.
88 S. R. S. Pralaharan, A. Fauzi, M. S. Michael and K. M. Begam, *Solid State Ionics*, 2004, **171**, 157.
89 D. Mikhailova, A. Sarapulova, A. Voss, A. Thomas, S. Oswald, D. M. Trots, N. N. Bramnik and H. Ehrenberg, *Chem. Mater.*, 2010, **22**, 3165.
90 X. J. Cui, S. H. Yu, L. L. Li, L. Biao, H. B. Li, M. S. Mo and X. M. Liu, *Chem. – Eur. J.*, 2004, **10**, 218.
91 P. Afanasiev, *J. Phys. Chem. B*, 2005, **109**, 18293.
92 V. I. Nefedov, M. N. Firsov and I. S. Shaplygin, *J. Electron Spectrosc. Relat. Phenom.*, 1982, **26**, 65.
93 K. Kuepper, I. Balasz, H. Hesse, A. Winiarski, K. C. Prince, M. Matteucci, D. Wett, R. Srargan, E. Burzo and M. Neumann, *Phys. Status Solidi A*, 2004, **201**(15), 3252.
94 K. G. Bramnik and H. Ehrenberg, *Z. Anorg. Allg. Chem.*, 2004, **630**, 1336.
95 A. A. Guarnieri, A. M. Moreira, C. B. Pinhiero and N. L. Speziali, *Physik*, 2003, **334**, 303.

96 S. C. Abrahams, J. L. Bernstein and P. B. Jamieson, *J. Chem. Phys.*, 1968, **48**(6), 2619.
97 L. Kihlborg and R. Norrestam, The symmetry of $Cu_3Mo_2O_9$, *Acta Crystallogr., Sect. B: Struct. Crystallogr. Cryst. Chem.*, 1972, 283097.
98 L. Katz, A. Kasenally and L. Kihlborg, *Acta Crystallogr., Sect. B: Struct. Crystallogr. Cryst. Chem.*, 1970, **27**, 2071.
99 V. V. Bakakin, R. F. Klevtsova and L. A. Gaponenko, *Kristallografiya*, 1990, **27**, 38.
100 S. C. Abrahams and J. M. Reddy, *J. Chem. Phys.*, 1965, **43**, 2533.
101 A. W. Sleight, B. L. Chamberland and J. F. Weiher, *Inorg. Chem.*, 1968, **7**, 1093.
102 G. W. Smith and J. A. Ibers, *Acta Crystallogr.*, 1965, **19**, 269.
103 R. M. Hazen, L. W. Finger and J. W. E. Mariathasan, *J. Phys. Chem. Solids*, 1985, **46**(2), 253.
104 A. K. Azad, S. G. Eriksson, S. A. Ivanov, R. Mathieu, P. Svedlindh, J. Eriksen and H. Rundlof, *J. Alloys Compd.*, 2004, **364**, 77.
105 V. Nassif, R. E. Carbonio and J. A. Alonso, *J. Solid State Chem.*, 1990, **146**, 266.
106 W. T. A. Harrison, A. K. Cheetham and J. Faber, *J. Solid State Chem.*, 1988, **76**, 328.
107 P. D. Battle, A. K. Cheetham, W. T. A. Harrison and J. Faber, *J. Solid State Chem.*, 1985, **58**, 221.
108 A. F. van den Elzen and G. D. Rieck, *Acta Crystallogr., Sect. B: Struct. Crystallogr. Cryst. Chem.*, 1973, **29**, 2436.
109 H.-Y. Chen and A. W. Sleight, *J. Solid State Chem.*, 1986, **63**, 70.
110 J. A. Alonso, F. Rivillas, M. J. Martinez-Lope and V. Pomjakushin, *J. Solid State Chem.*, 2004, **177**, 2470.
111 M. Ozima, S. Sato and T. Zoltai, *Acta Crystallogr., Sect. B: Struct. Crystallogr. Cryst. Chem.*, 1977, **33**, 2175.
112 B. M. Gatehouse and P. Leverett, *J. Solid State Chem.*, 1970, **1**, 484.
113 J. P. Badaud, J. P. Fournier and J. Omaly, *C. R. Acad. Sci. C*, 1977, **284**, 921.
114 F. Theobald and A. Laarif, *Mater. Res. Bull.*, 1985, **20**, 653.
115 A. Arulraj, K. Ramesha, J. Gopalakrishnan and C. N. R. Rao, *J. Solid State Chem.*, 2000, **155**, 233.
116 V. V. Atuchin, O. Y. Khyzhun, O. D. Chimitova, M. S. Molokeev, T. A. Gavrilova, B. G. Bazarov and J. G. Bazarova, *J. Phys. Chem. Solids*, 2015, **77**, 101.
117 V. V. Atuchin, E. N. Galashov, O. Yu. Khyzhun, A. S. Kozhukhov, L. D. Pokrovsky and V. N. Shlegel, *Cryst. Growth Des.*, 2011, **11**, 2479.
118 V. V. Atuchin, M. S. Molokeev, G. Yu. Yurkin, T. A. Gavrilova, V. G. Kesler, N. M. Laptash, I. N. Flerov and G. S. Patrin, *J. Phys. Chem. C*, 2012, **116**, 10162.
119 M. D. Faucher and P. A. Tanner, *J. Phys.: Condens. Matter*, 2006, **18**, 8503.
120 S. P. Keller and G. D. Petit, *Phys. Rev.*, 1961, **121**, 1639.
121 S. Sakirzanovas, A. Katelnikovas, H. Bettentrup, A. Kareiva and T. Justel, *J. Lumin.*, 2011, **131**, 1525.